Chapter 3

Floquet analysis of a system with fractal spectrum

3.1 Introduction

Even before the recent spurt of activities in the study of Floquet systems, the periodically driven classical and quantum systems are studied extensively in the field of classical and quantum chaos [34, 79–81]. Chaos is a well defined property of a classically nonintegrable system: classical systems, which show sensitivity to the initial conditions, are called chaotic systems. Heisenberg's uncertainty principle does not allow to translate this classical definition in to the quantum domain. One can only look for certain signatures in quantum systems whose underlying classical dynamics are chaotic. For the periodically time dependent systems, the quasienergy spectrum shows certain statistical signatures that are different from the spectral property of any non-chaotic system. This is known as the Bohigas-Giannoni-Schmit (BGS) conjecture [82]. Recently, few such nonintegrable systems have also been studied from the Floquet theory perspective [38, 54]. However, there is a class of periodically driven systems whose underlying classical dynamics is chaotic, but

their spectrum does not follow the BGS conjecture. Periodically δ-kicked Harper model [83–88] and its variants [87, 88] are examples of this class of dynamical systems. The quasienergy spectrum of these systems shows a nice 'butterfly' like fractal spectrum. This is an exceptional property that indicates the possibility of an infinite number of quantum phase transitions [89]. This kind of butterfly spectrum was also observed in the time independent version of the Harper model [64]. This model describes a system of free electrons moving on two dimensions and subjected to a square lattice potential with a perpendicular magnetic field [64,90]. It is found that the spectrum of this system shows fractal behavior for any irrational value of a system parameter (magnetic flux quanta) [91, 92].

Recently, a new driving scheme is developed under which some other class of dynamical systems have also shown a fractal spectrum. This new driving scheme is the combination of two δ-kicks, separated by a finite time interval, acting on the system within a single time period T; and the polarity of the two kicks are opposite to each other. The single kicked rotor and the single kicked top are two well known models that are classically chaotic, and their quasienergy spectrum also follows the BGS conjecture. However, when one drives these systems under the above mentioned double δ-kicked schemes, then in certain parameter regimes, the quasienergy spectrum of these systems show fractal property [55–58].

The Floquet analysis of the single kicked top is done recently [54] following the perturbation theory proposed in [26, 27]. We now focus on the Floquet analysis of the double-kicked top (DKT) system. Following our discussion in earlier chapters, here we like to compute the effective time independent Hamiltonian or the Floquet Hamiltonian of the system. Then we extensively study the fractal property of the spectrum of this system from different perspectives.

Section 3.2 introduces the DKT model and discusses its properties. In this section, the effective Hamiltonian is also calculated by applying perturbation theory. The next two sections 3.3 and 3.4 discuss the different aspects of the fractal properties in the quasienergy spectrum. The self-similar property of the quasienergy spectrum is discussed in Sec. 3.5. Finally, a conclusion is drawn in Sec. 3.6.

3.2 Model

We focus here to study the Floquet Hamiltonian of the DKT model. The Hamiltonian of the DKT model is given as:

$$\begin{aligned} H &= \frac{2\alpha}{T} J_x + \frac{\eta}{2j} J_z^2 \sum_{n=-\infty}^{\infty} \Big[\delta(t - nT + T/2) - \delta(t - nT)\Big], \\ &= H_0 \, + \, V \, F(t), \end{aligned} \tag{3.1}$$

where the undriven part $H_0 = \frac{2\alpha}{T} J_x$, the driven part $V = \frac{\eta}{2j} J_z^2$, and

$$F(t) = \sum_{n=-\infty}^{\infty} \Big[\delta(t - nT + T/2) - \delta(t - nT)\Big],$$

describes the driving scheme. A schematic diagram of the driving scheme is shown in Fig. 3.1: Here the dimension of Hilbert space is $d = 2j + 1$, and J_i represents the angular momentum operators. In the Hamiltonian, the time independent term describes a rotation about the x-axis with angle α within a time period T. The time dependent driven term appearing stroboscopically twice within a time period T and each time gives a twist about the z-axis of strength η, but acts in opposite directions as shown in Fig. 3.1. The corresponding time evolution operator over

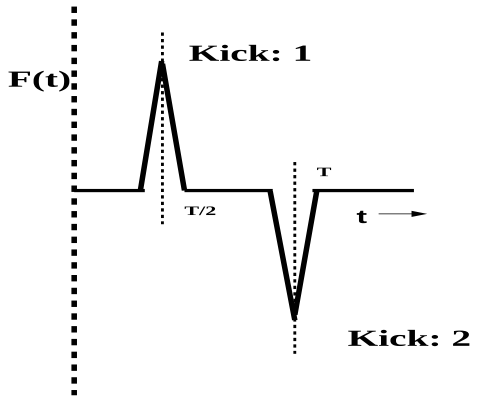

FIGURE 3.1: Driving scheme is shown for one time period T. The two kicks are acting in opposite directions. This scheme repeat itself in every time period between nT to $(n+1)T$

.

one period or the Floquet operator is:

$$\mathcal{F} = \exp(-i\alpha J_x)\exp\left(-i\frac{\eta}{2j}J_z^2\right)\exp(-i\alpha J_x)\exp\left(i\frac{\eta}{2j}J_z^2\right). \tag{3.2}$$

The Floquet operator is a product of four unitary operators. However, this operator can also be written as a product of two unitary operators as:

$$\mathcal{F} = \exp(-i\alpha J_x)\exp\big[-i\alpha J_+\{e^{i\frac{\eta}{2j}(2J_z+\mathbb{1})}\} + \text{h.c.}\big]. \tag{3.3}$$

The detail derivation of this is presented in Appendix B.1. Here, $J_\pm = (J_x \pm iJ_y)/2$ are the ladder operators. The later form of the Floquet operator, can also be obtained from an equivalent single kicked Hamiltonian of the form

$$H = H_0 + V\sum_{n=-\infty}^{\infty}\delta(t-nT), \tag{3.4}$$

where

$$V = \alpha J_x \quad \text{and} \quad H_0 = \alpha\frac{J_+}{T}\exp\left[i\frac{\eta}{2j}(2J_z+\mathbb{1})\right] + \text{h.c.} \tag{3.5}$$

Instead of the DKT model, we can now study its equivalent single kicked model. This gives us freedom to apply directly the expression derived in Eq. (2.29) for the effective Hamiltonian at the high-frequency limit for the generic single kicked system up to an order of ω^{-2}:

$$H_{\text{eff}} = H_0 + \frac{V}{T} + \frac{1}{24}\big[[V, H_0], V\big] + \mathcal{O}\left(\frac{1}{\omega^3}\right).$$

3.2.1 Symmetries in the DKT model

We are interested in investigating the spectral properties of this effective Hamiltonian H_{eff}. The original time dependent Hamiltonian H has the following unitary symmetry:

$$R_x^\dagger\left(\frac{\pi}{2}\right) H R_x\left(\frac{\pi}{2}\right) = H, \tag{3.6}$$

where

$$R_x\left(\frac{\pi}{2}\right) = e^{-i\frac{\pi}{2}J_x}. \tag{3.7}$$

We find that the effective time independent Hamiltonian H_{eff} also carries the same unitary symmetry. However, the original time dependent Hamiltonian H had an additional unitary symmetry for $\frac{\alpha}{T} = \frac{\pi}{4}$, this additional symmetry will never appear in the effective Hamiltonian because we consider here much smaller values of $\frac{\alpha}{T}$.

Since a unitary symmetry preserved in H_{eff}, we consider the corresponding symmetry reduced basis in which the effective Hamiltonian will be block-diagonal $H_{\text{eff}} = H_{\text{eff}}^{\text{even}} \oplus H_{\text{eff}}^{\text{odd}}$. We define these bases as the *even* and *odd* [93]:

$$\text{Even}: \left\{ |0\rangle, \frac{1}{\sqrt{2}}\big(|2m\rangle + |-2m\rangle\big), \frac{1}{\sqrt{2}}\big(|2m-1\rangle - |1-2m\rangle\big) \right\} \text{of dimension } j+1;$$
$$\text{Odd}: \left\{ \frac{1}{\sqrt{2}}\big(|2m\rangle - |-2m\rangle\big), \frac{1}{\sqrt{2}}\big(|2m-1\rangle + |1-2m\rangle\big) \right\} \text{of dimension } j,$$

where $m = 1, ..., j/2$, and hence we restrict ourselves for j equals to any even integer. The size of the even block is $j + 1$ and and the odd block is j. We denote this symmetry reduced by $\{|\overline{m}\rangle\}$. These two blocks are dynamically independent because they represent two invariant subspaces of H_{eff}. Therefore, we can study the spectral properties of these two subspaces independently, and they are expected to show qualitatively similar behavior. We have verified this fact by our numeric. Here, we are now showing the results obtained in the even subspace.

3.3 Result

We now discuss details of the properties of energy eigenvalues and eigenstates of the effective Hamiltonian corresponding to the DKT model.

3.3.1 Properties of Eigenvalues

Fig. 3.2 shows the energy spectrum of the effective Hamiltonian H_{eff} as a function of $\xi = \eta/2\pi j$ for $\alpha = 1/j$ folded within the original range $[-\pi, \pi]$. Here, we set $j = 20$, an even number. We find that the eigen spectrum of the effective Hamiltonian also shows a differently looking butterfly like spectrum, which is in a good agreement with the quasienergy spectrum of the original DKT model [55, 57]. This eigen spectrum of the effective Hamiltonian shows qualitative similarity with the Hofstadter butterfly [64] owing to the presence of quasiperiodic term. The DKT butterfly is different from the Harper-Hofstadter butterfly, because the quasiperiodic term is present along the diagonal of the Harper-Hofstadter case; whereas in the DKT case this term is present along the off-diagonal nearest neighbor band.

In order to investigate the multifractality in the energy spectrum, we set η/j at the golden mean ratio $G_r = \frac{\sqrt{5}-1}{2}$, the *most* irrational number. Since here we are

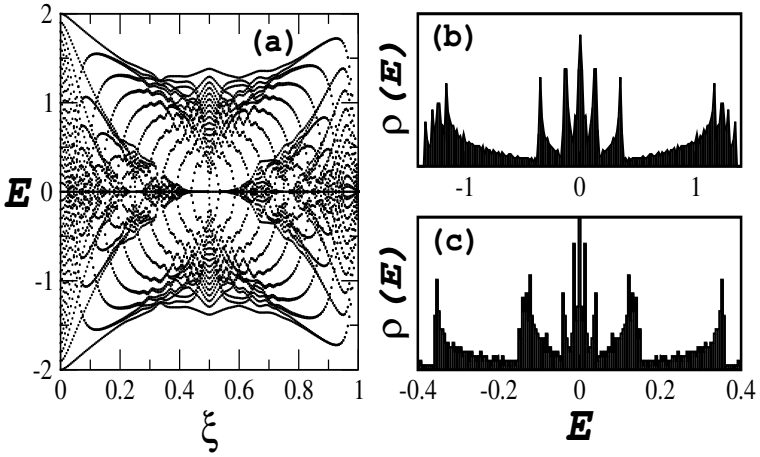

FIGURE 3.2: (a) The energy spectrum of the effective Hamiltonian of the DKT folded in the first Floquet Brillouin zone is presented. The spectrum is showing the butterfly pattern. (b)-(c) Self-similarity in the DOS of the energy spectrum is shown by zooming on different scales, Here we set $\xi = G_r/2\pi$, where $G_r = \frac{\sqrt{5}-1}{2}$ is the golden mean ratio, the "most irrational number."

interested in the property of the spectrum for a fixed parameter value, we consider j equals to a large even number $j = 2500$. The multifractality is a generalization of the fractal property, where a continuous spectrum of exponents is required to describe the data. The multifractal patterns are scale-dependent, whereas the fractal patterns are independent of any scale. In Fig. 3.2(b) and 3.2(c), we have investigated the density of states $\rho(E)$ at two different scales. This figure exhibits self-similarity in the density of states (DOS) at two different scales. The self-similar property of the whole spectrum will be discussed more elaborately later.

3.3.2 Properties of the eigenstates

We now study the eigenstates of the effective Hamiltonian H_{eff}. At the top panel of Fig. 3.3, we have presented the participation ratio (PR) of all the eigenstates as a function of their eigenvalues E. The PR measures the localization or delocalization of any quantum state in a given basis. The PR gives a measure of how many basis states are participating to construct the given quantum state. Therefore, if the

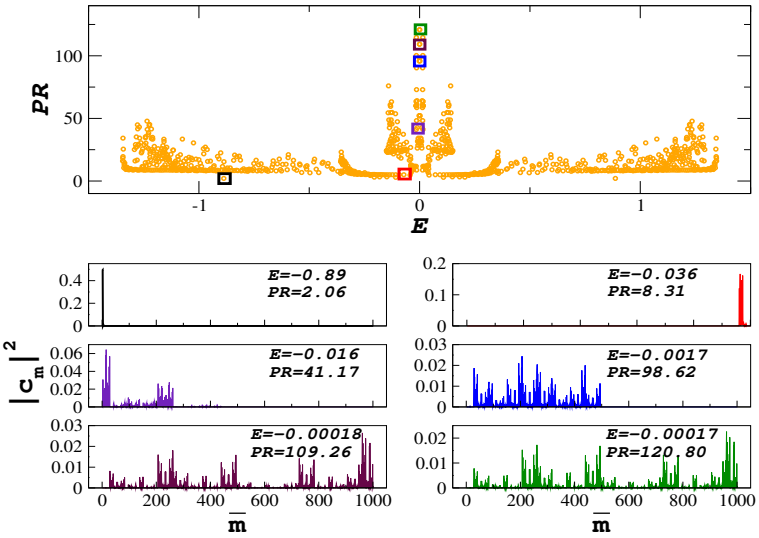

FIGURE 3.3: The top panel shows the PR values of all the eigenstates. Remaining lower panels show the selected six eigenstates with their energy values and the PR values.

PR is large (small), the state is delocalized (localized) in the given basis. Here, the PR is calculated in the symmetry reduced basis $\{|\overline{m}\rangle\}$. Mathematically, if an eigenstate is expanded in the $\{|\overline{m}\rangle\}$ basis as $|\psi\rangle = \sum_{\overline{m}} C_{\overline{m}} |\overline{m}\rangle$, then the PR of this state will be $1/\sum_{\overline{m}} |C_{\overline{m}}|^4$. We have selected *six* eigenstates based on their PR values, marked by colored square boxes in the top panel of Fig. 3.3, and presented them in the lower panels. Among the six selected states, one of the eigenstates with energy $E = -0.89$ shown in black color has very sharp support over a narrow band of basis states around $|\overline{m}\rangle = 1$. This indicates that the eigenstate is highly localized. The PR for this eigenstate is 2.06, which suggests that approximately only two or three basis states have major participation or contribution to this state. Remaining five selected eigenstates have $E = -0.036$ with $PR = 8.31$, $E = -0.016$ with $PR = 41.17$, $E = -0.0017$ with $PR = 98.62$, $E = -0.00018$ with $PR = 109.26$ and $E = -0.00017$ with $PR = 120.80$. The eigenstate with $PR = 120.80$ is shown by green color, which is the most delocalized state among all the eigenstates. We are working in the even subspace of dimension $j + 1 = 1001$. In comparison to the dimension of this subspace, the largest value of the PR (~ 121) is much smaller.

The maximum possible value of the PR is equal to the subspace dimension 1001. This value of PR is possible when all the components of the eigenstate will be equal to $1/\sqrt{j+1} = 1/\sqrt{1001}$. Thus we observe that, in comparison to the maximally delocalized state, all the eigenstates of the effective Hamiltonian H_{eff} are very much localized.

We are now interested in exploring the multifractal property of these selected eigenstates. This property is studied by computing the generalized fractal dimension D_q using the standard box-counting method [94]. We divide the total dimension $d = j + 1$ of the even subspace into M_l pieces or boxes of linear size $l \sim d/M_l$ and denote the components of the n-th eigenstate as $\{C_{\overline{m}}^{(n)}\}$. The box probability of the eigenstate in the i-th box is defined as:

$$\widetilde{p}_i(l) = \sum_{\overline{m} \in i\text{-th box}} |C_{\overline{m}}^{(n)}|^2, \tag{3.8}$$

where the summation extends over the components $C_{\overline{m}}$ in the i-th box. Now we calculate the q-th moment of this measure, over all the boxes and determine

$$\chi_q(l) = \sum_i \widetilde{p}_i(l)^q. \tag{3.9}$$

An eigenstate to be multifractal, its $\chi_q(l)$ is proportional to some power of τ_q for the box of size l, where τ_q is called the scaling exponent. We can calculate the general fractal dimension $\overline{D}_q$ from the following relation:

$$-\tau_q = (q-1)\overline{D}_q = \lim_{l \to 0} \frac{\ln \chi_q(l)}{\ln l}, \tag{3.10}$$

where the parameter q can be any real value according to the definition of $\overline{D}_q$. We are restricting us in the region where $q \geq 0$. This is because, for the positive values

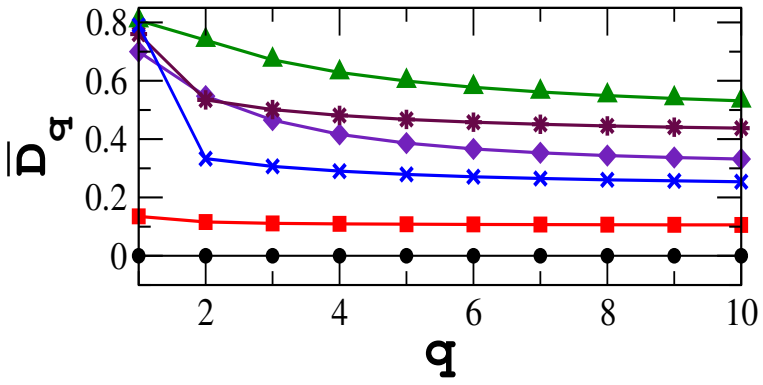

FIGURE 3.4: Generalized fractal dimension $\overline{D}_q$ as a function of q is shown for the selected eigenstates. The top four eigenstates are showing strong sensitivity with the scaling parameter q. This indicates multifractal property of the eigenstates. The following two states show almost no dependence on the scaling parameter q. These two states are localized states with very small values of the PR.

of q, the larger components of eigenstates determines $\overline{D}_q$. On the other hand, the negative values of q determine the smaller components of the eigenstates that play a significant role in determining $\overline{D}_q$. Though the smaller components of the eigenstates are susceptible to the numerical errors, and as a result, the calculated values of $\overline{D}_q$ for the negative values of q will be erroneous.

In Fig. 3.4, we have presented the multifractal property of eigenstates by presenting the generalized fractal dimension $\overline{D}_q$ as a function of the scaling parameter q. The top four eigenstates, presented in green, maroon, blue, and purple colors with PR values $120.80, 109.26, 98.62$, and 41.17, respectively, show stronger sensitivity to the scaling parameter q. This also suggests a stronger multifractal nature of these eigenstates. The next two selected eigenstates drawn in red and black colors show almost no dependence on the scaling parameter q. These two states are more localized than the previous four states, as their PR values are 8.31 and 2.06, respectively. Following our expectation, the generalized fractal dimension $\overline{D}_q$ of the most localized state (drawn in black color) is equal to zero, and thus it is completely independent for all the values of the scaling parameter q. The moderately localized state shows a very weak dependence on the scaling parameter q.

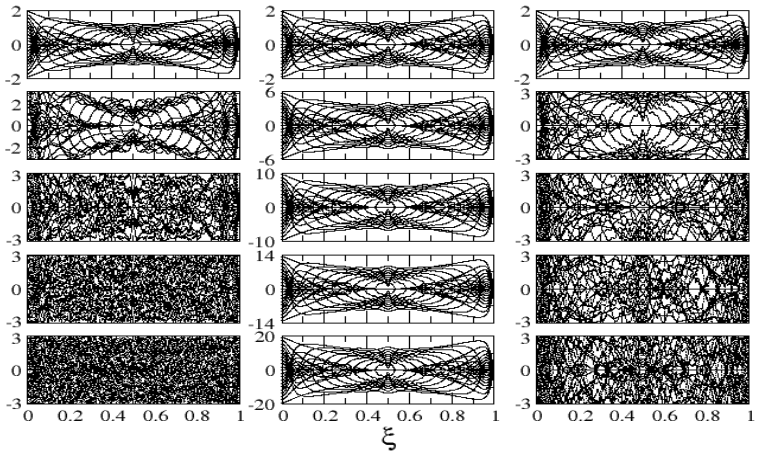

FIGURE 3.5: Disappearance of the DKT butterfly is shown for different values of $\alpha = n/j$, where $n = 1, 3, 5$ and 10 from top to bottom and $j = 20$. The left and right columns show the quasienergy spectrum of the Floquet time-evolution operator and the energy spectrum of the Floquet Hamiltonian folded in the first Floquet-Brillouin zone, respectively. We see here how the butterfly is disappearing as we increase the parameter α. The central column shows the unfolded energy spectrum of the Floquet Hamiltonian, where we do not observe any disappearance of the butterfly. However, the size of the butterfly increases with the increment of the parameter α.

Fig. 3.4, shows a general feature that the eigenstates with larger PR values show stronger sensitivity to the scaling parameter q, which also indicates their stronger multifractality.

3.4 Disappearance of the butterfly

From the earlier studies, it is known that the quasienergy butterfly spectrum of the Floquet operator of DKT gradually disappears by increasing parameter α [55]. In Fig. 3.5, we have shown the quasienergy spectrum of the Floquet time evolution operator at the left column, the unfolded energy spectrum of the effective Hamiltonian at the central column, and the energy spectrum of effective Hamiltonian H_{eff} folded in the first Floquet-Brillouin zone at the right column.

In the left and right column, we observe the disappearance of the butterfly with the increment of α, where $\alpha = n/j$ and $n = 1, 3, 5$ and 10 with $j = 20$. As

we increase the parameter α, we notice the deformation in the butterfly of the quasienergy spectrum. Eventually, for a larger value of α we see the complete disappearance of the butterfly. The same was also reported in Ref. [55].

At the center column of Fig. 3.5, we have presented the unfolded energy spectrum of the effective Hamiltonian H_{eff}. Here again, we consider the same values of α, which we have selected for the quasienergy spectrum of the Floquet operator. Here, we do not see any disappearance of the butterfly, but the butterfly's enlargement is noticed with the increment of parameter α. This is because the effective Hamiltonian H_{eff} mainly has two parts, where one part has the form $H_0 + V$ which is directly proportional to α and another part has the form $\frac{1}{24}[[V, H_0], V]$, which is quadratically dependent on α. Here we have considered very small values of α of the order of $1/j$; as a consequence, the effective Hamiltonian H_{eff} becomes directly proportional to the parameter α. As a consequence, the size of the butterfly increases linearly with an increasing value of α. We can project any two spectra with different values of α on the top of each other just by dividing or multiplying the spectrum with the proper scaling factor. This suggests that if we divide the spectrum corresponding to $\alpha = n/j$ by the factor n, where $n > 1$, then the entire spectrum can be projected exactly on the spectrum corresponding to $\alpha = 1/j$.

The right column of Fig. 3.5, shows the result for the energy spectrum of the effective Hamiltonian folded into the first Floquet-Brillouin zone. Here we observe the disappearance of the butterfly with increment in α. The behavior of the folded energy spectrum of H_{eff} as a function of α is expected to behave similarly to the quasienergy spectrum of the Floquet operator. Here we observe a slight difference between the quasienergy spectrum and the folded energy spectrum for larger values of $\alpha = n/j$ with $n = 3, 5, 7$, and 10. This is due to the truncation effect at $1/\omega^2$.

We now investigate the DOS $\rho(E)$ of the folded eigenvalues of the effective

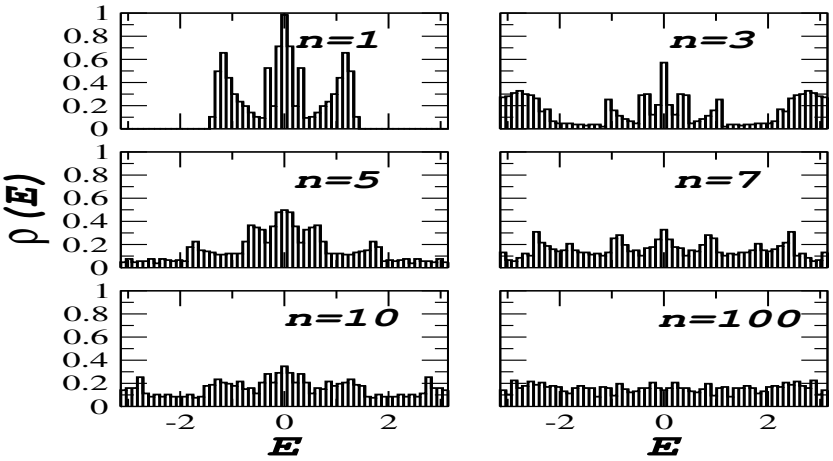

FIGURE 3.6: The DOS of the folded energy eigenvalue of the effective Hamiltonian is shown for $\alpha = n/j$. Here $n = 1, 3, 5, 7, 10$ and 100 for a very large value of $j = 2500$ is considered.

Hamiltonian H_{eff} as a function of α for a fixed value of η/j. Here we set η/j equals π times the Golden mean ratio. We also set a large value of spin $j = 2500$ to obtain a good statistic of the density of state (DOS). In Fig. 3.6, we have shown DOS $\rho(E)$ for $\alpha = n/j$ with $n = 1, 3, 5, 7, 10$ and 100. We have already shown the result for $n = 1$ and $\alpha = 1/j$ in Fig. 3.2(b). Here we are interested in showing how $\rho(E)$ changes with α. For $n = 3$, the energy spectrum spread up to the end of the first Floquet-Brillouin zone $|E| = \pi$. For the same value, the central band of the spectrum for the range $|E| \leq 0.4$ still shows the property of self-similarity. In Fig. 3.6, we observe that for further increment in α by varying n from 3 to $5, 7$, and 10, the self-similar part of the energy spectrum, located around the central part, gradually disappears. For $n = 100$, $\alpha = 100/j$, which is sufficiently large in magnitude, we observe a complete disappearance of the self-similar part in the energy spectrum. At this large value of α, $\rho(E)$ is approximately flat, and we conclude a uniform distribution of the energy spectrum.

3.5 Fractal and self-similarity of the DKT spectrum

Hofstadter butterfly is a well known quantum spectrum which shows a self-similar fractal property. This spectrum was obtained for a system of noninteracting free electrons moving in a two-dimensional surface under the presence of a magnetic field perpendicular to the surface [64]. The butterfly pattern is observed when the energy spectrum is plotted as a function of the magnetic flux strength. The fractal property and also the self-similar property of the Hofstadter butterfly are generally studied for some specific values of the magnetic flux strength. Recently, these properties are studied considering the whole butterfly as a single object.

In the case of the DKT model, the parameter ξ plays the role of the magnetic flux. All the previous studies of the DKT also focused mostly on some specific values of ξ [55–57]. In the previous section, we have discussed the DKT spectrum's self-similarity for a specific value of parameter $\eta/j = G_r$ or $\xi = G_r/2\pi$, where G_r is the golden mean ratio. Now, we study the fractal property and the self-similar property of the whole DKT butterfly spectrum.

3.5.1 Fractal properties

In the previous section, the DKT butterfly's disappearance is observed with the increment of the parameter α. We now explore how the fractal property of the whole butterfly, observed in the quasienergy spectrum and as well as in the energy spectrum of the effective Hamiltonian H_{eff}, change with the parameter α. Here we assume that the butterfly is lying on a two-dimensional surface, which is formed by the parameter $\xi = \eta/2\pi j$ and the quasienergy/energy spectrum. We calculate the fractal dimension D_2 of the whole DKT butterfly by the box-counting method [95].

We divide the whole butterfly, which is lying on a two-dimensional surface into many square boxes or partitions, and then counts the number of points of the butterfly in each of the boxes. We can choose the total number of points required to construct the butterfly by setting the spin j and the number of divisions along the ξ direction within the range of $0 \leq \xi \leq 1$. We set the spin $j = 20$ at an even value and vary the parameter ξ from 0 to 1 in 1000 steps. Therefore the total number of points are used to construct the butterfly in the even parity subspace is $(j+1) \times 1000 = 21000$. Using this number, we can assign the box probability of the individual boxes and then calculate the fractal dimension D_2 by the box-counting method.

We have observed butterfly in the exact quasienergy spectrum and also in the energy spectrum of the effective Hamiltonian H_{eff} at $\alpha = 1/j$ with $j = 20$. These two butterflies look very much identical, at least to the naked eyes. However, they are not exactly identical, which we see from the fractal dimension D_2. We observe that the fractal dimension of theses two butterflies is not equal. For the quasienergy spectrum, the fractal dimension $D_2 \simeq 1.35$, whereas for the energy spectrum of effective Hamiltonian $D_2 \simeq 1.76$. This indicates that these two butterflies have some *minute* differences.

In Fig. 3.7, we have shown the variation of fractal dimension D_2 with the parameter α for both the butterflies. The results for the quasienergy spectrum have shown by the blue color line with solid circles. As we increase the value of α from 0 to π, we observe that D_2 reaches maximum at $\alpha = \pi/2$. Further increment in α, the fractal dimension D_2 starts decreasing and reaches its minimum value at $\alpha = \pi$. After that we see the repetitions of the same behavior. The fractal dimension D_2 reaches its maximum value at $\alpha = (2m+1)\pi/2$ and minimum value $D_2 = 1.0$ at $\alpha = m\pi$, where $m = 0, 1, 2, 3, ...$ Here, we have not shown the trivial

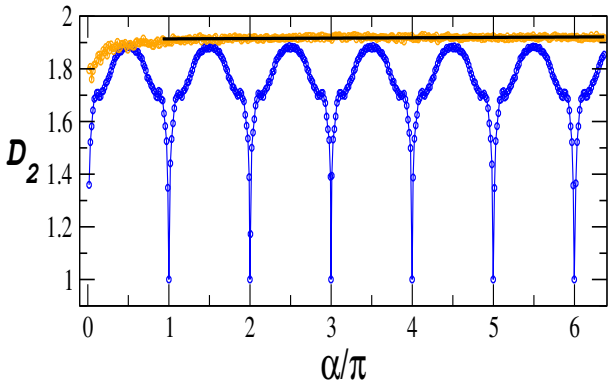

FIGURE 3.7: The variation of fractal dimension D_2 with parameter α for the butterfly formed by the quasienergy spectrum shown by blue color circles and by the folded energy eigenvalue E of the effective Hamiltonian shown by orange color circles. The solid black line shows that D_2 of the butterfly formed by the folded energy spectrum increases continuously in a linear fashion with the slope of the order of 10^{-3}. It reaches asymptotically at $D_2 = 2.0$ (Euclidean dimension of the parameter space "ξ-E") as a function of α.

case of $\alpha = 0$, which we get for $m = 0$.

The periodic behavior in the fractal dimension D_2, as a function of α, can be understood by replacing $\alpha \to \alpha + m\pi$ in the expression of the Floquet time evolution operator. For any integer value of m, the Floquet operator $\mathcal{F}$ remains the same. Therefore, the whole quasienergy spectrum between $0 \leq \xi \leq 1$ repeat itself for every interval of $m\pi \leq \alpha \leq (m+1)\pi$. As a result, we can see an identical butterfly for all values of $\alpha + m\pi = \frac{1}{j} + m\pi$. At $\alpha = m\pi$, the Floquet time evolution operator becomes an *identity* operator, and we observe the minima in fractal dimension D_2. Consequently, all the quasienergies in the first Floquet-Brillouin zone become degenerate at $\epsilon = 0$ for all values of ξ and form a straight line on the $\xi - E$ plane. The fractal dimension D_2 becomes equal to the dimension of the straight line, i.e., $D_2 = 1.0$.

This property of quantum resonance at $\alpha = m\pi$ for the Floquet operator is not observed in the effective Hamiltonian energy spectrum. In Fig. 3.7, the variation of fractal dimension D_2 as a function of α for the energy spectrum of H_{eff} is shown by orange solid circles. For this curve, we obtain a straight-line fitting for the region

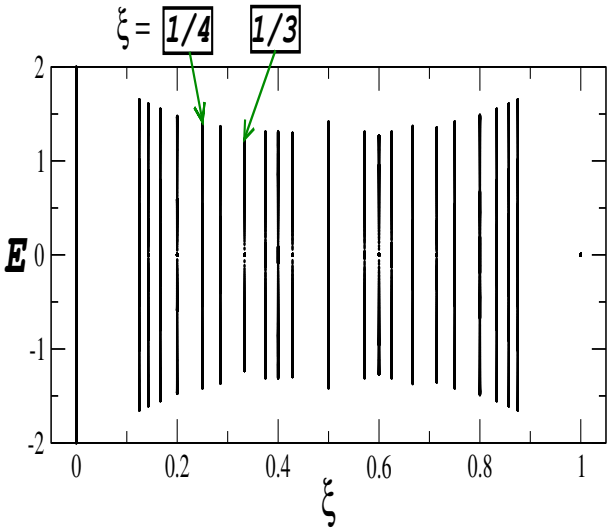

FIGURE 3.8: Skeleton of the DKT butterfly is shown for a set of rational values for the parameter ξ in the range [0,1]. We use these rational numbers from Farey sequence of order 8.

$\alpha \geq \pi$. This straight line has a small but positive slope of the order of 10^{-3}. As a result, we observe a steady increment in fractal dimension D_2 as a function of α and is asymptotically approaching towards the value 2.0, which is nothing but the Euclidean dimension of the "$\xi - E$" plane where the whole spectrum is lying.

3.5.2 Self Similarity: "Butterfly at every scale"

A pattern is called self-similar if it is exactly similar to some part of itself or if it repeats itself at every scale. Following Ref. [96, 97], we now analyze the self-similar property of the DKT butterfly from the geometrical and number theoretical aspects. This analysis is originally performed to investigate the fractal properties of the Hofstadter butterfly. Here we are interested in performing the same analysis on the DKT butterfly. These two butterflies are clearly not identical. The wings of the Hofstadter butterfly are empty, representing gaps in the spectrum, whereas the wings of the DKT butterfly are not empty and form a gapless spectrum, as shown in Fig. 3.2(a). Figures 3.2(b) and 3.2(c) also confirm the gapless spectrum, where the DOS is continuous without any gap.

We start the investigation of the self-similar property of the DKT butterfly, considering only rational values of the parameter ξ. We construct these rational values between $[0, 1]$ from the Farey sequence [98]. The sequence of rational numbers F_8, the Farey sequence of order 8 (which is given in Sec. B.2) construct the skeleton or the basic structure of the DKT butterfly as shown in Fig. 3.8.

For the Hofstadter butterfly, at a fixed rational value of the magnetic flux, i.e., $\phi = \frac{p}{q}$, the spectrum has q bands and $(q-1)$ gaps [96]. It is also shown that, for the even values of q, the two central bands touch each other, and that results in the observed $(q-2)$ bands. However, we do not observe such distinct band gaps in the DKT spectrum for different rational values of ξ. In Ref. [96], the Hofstadter butterfly is represented by p/q rational value of magnetic flux. For this fixed value of magnetic flux strength ϕ, there are q bands and $(q-1)$ gaps. It is also mentioned that, for an even value of q, the two central band touch each other. As a result, the number of observed bands is $(q-2)$. Here in the case of DKT, we do not see such distinct band gaps for different rational values of ξ. Fig. 3.8 shows a continuous spectrum both at $\xi = 1/4$ (q is even) and $\xi = 1/3$ (q is odd). For both, these values of q, *two* gaps were found in Hofstadter butterfly.

We now investigate the behavior of the butterfly at the vicinity of $\xi = 1/4$ and $\xi = 1/3$. This part of the DKT butterfly is presented in Fig. 3.9. The rational value of ξ with even denominator always forms the center of a butterfly. For example, $\xi = \frac{1}{2}$ forms the center of the biggest butterfly having range between $\xi = 0$ to $\xi = 1$. Similarly, $\xi = \frac{1}{4}$ forms the center of a smaller butterfly. The region around the odd denominator case, the behavior of spectrum, is completely different. Around $\xi = \frac{1}{3}$, we see a boundary that separates a proliferation of nested butterflies. In the case of the Hofstadter butterfly, left and right symmetry around $\phi = 1/3$ was observed for this same value of the magnetic flux. However, in the case of the DKT, such

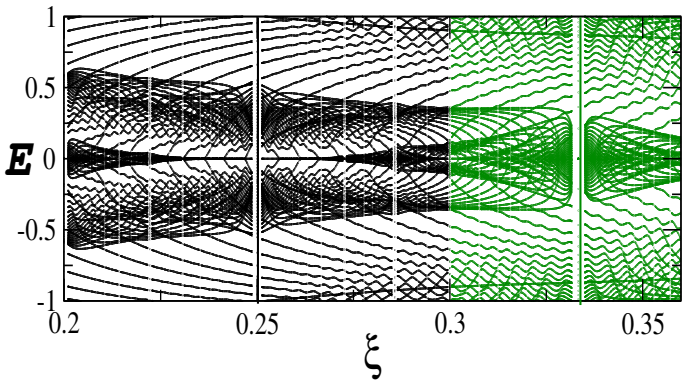

FIGURE 3.9: Some part of DKT butterfly is shown in the area of $\xi = 1/4$ (black colored region) and $\xi = 1/3$ (green colored region).

left and right symmetry is absent.

Following Ref. [96], we now explore the self-similar property of the DKT butterfly spectrum at different scales. As we zoom in the main butterfly, we observe another butterfly, and this process goes on at every scale. All these butterflies at different scales share minute details of the original butterfly. The butterflies observed at different scales are called the generations of butterflies.

Each of such butterfly is represented by a triplet $(\xi_L = \frac{p_L}{q_L}, \xi_C = \frac{p_C}{q_C}, \xi_R = \frac{p_R}{q_R})$ of rational numbers. Here $\xi_L = \frac{p_L}{q_L}$ and $\xi_R = \frac{p_R}{q_R}$ are left and right edges of the butterflies and $\xi_C = \frac{p_C}{q_C}$ is the center. These triplets are connected to each other by the following relation:

$$\frac{p_C}{q_C} = \frac{p_L + p_R}{q_L + q_R} \equiv \frac{p_L}{q_L} \oplus \frac{p_R}{q_R}. \tag{3.11}$$

The above relation is known as the Farey sum [98]. According to the definition of generations, the first generation of the butterfly or the parent butterfly is the full butterfly stretching from $\xi = 0$ to 1. Here we consider the case where the larger and the smaller butterflies share neither their left edge nor their right edge. These different generation butterflies are obtained as usual by zooming the butterfly of the previous generation. The recursive scheme which connects the two successive

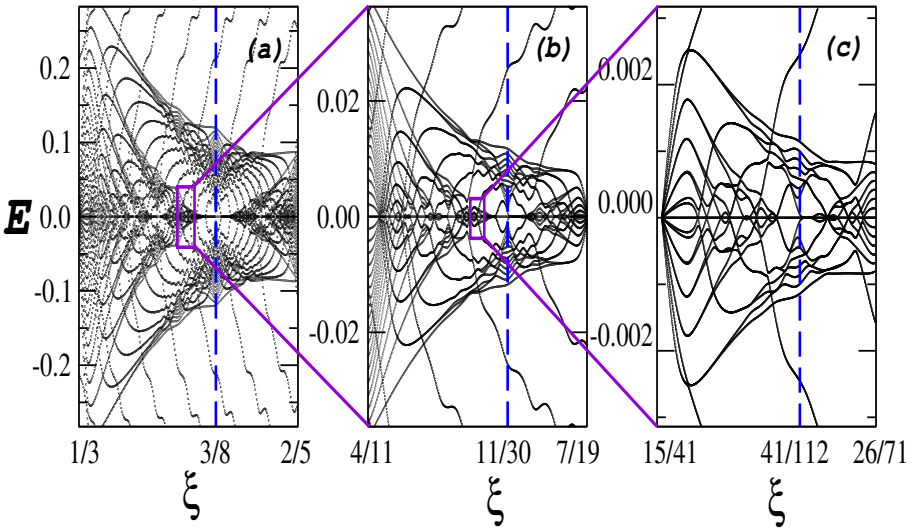

FIGURE 3.10: Successive generations of butterflies are shown. These butterflies show self-similarity in the folded energy spectrum of the effective Hamiltonian of DKT. The range of figures are (a) $\xi = \frac{1}{3}$ to $\xi = \frac{2}{5}$, (b) $\xi = \frac{4}{11}$ to $\xi = \frac{7}{19}$ and (c) $\xi = \frac{15}{41}$ to $\xi = \frac{26}{71}$.

generations of the butterfly is given in [96]:

$$\begin{aligned} \xi_L(l+1) &= \xi_L(l) \oplus \xi_C(l), \\ \xi_R(l+1) &= \xi_L(l+1) \oplus \xi_C(l), \\ \xi_C(l+1) &= \xi_L(l+1) \oplus \xi_R(l+1), \end{aligned} \tag{3.12}$$

where l and $l+1$ represent the successive generations. We have shown the main butterfly or the first generation butterfly in Fig. 3.2(a). For this butterfly $\xi_L = \frac{0}{1}$, $\xi_R = \frac{1}{1}$ and $\xi_C = \frac{1}{2}$. Now in Fig. 3.10, we represent the three successive generations of butterflies.

In Fig. 3.10(a), the second generation of the DKT butterfly is shown. This butterfly has the left edge at $\xi_L(l+1) = \frac{0}{1} \oplus \frac{1}{2} = \frac{1}{3}$ and the right edge at $\xi_R(l+1) = \frac{1}{3} \oplus \frac{1}{2} = \frac{2}{5}$. The center of the butterfly is at $\xi_C = \frac{1}{3} \oplus \frac{2}{5} = \frac{3}{8}$. Therefore, the second generation of butterfly is represented by a triplet $(\frac{1}{3}, \frac{2}{5}, \frac{3}{8})$.

In a similar way, another triplet is required to represent the next generation butterfly. This we obtain from the previous generation by the following way: the

left edge is at $\xi_L(l+2) = \xi_L(l+1) \oplus \xi_C(l+1) = \frac{1}{3} \oplus \frac{3}{8} = \frac{4}{11}$, the right edge is at $\xi_R(l+2) = \xi_L(l+2) \oplus \xi_C(l+1) = \frac{4}{11} \oplus \frac{3}{8} = \frac{7}{19}$, and the center part is at $\xi_C(l+2) = \xi_L(l+2) \oplus \xi_R(l+2) = \frac{4}{11} \oplus \frac{7}{19} = \frac{11}{30}$. The butterfly of this generation is represented by the triplet $(\frac{4}{11}, \frac{7}{19}, \frac{11}{30})$ and this is shown in Fig. 3.10(b). Following identical procedure, we get the next generation butterfly and represent that by the triplet $(\frac{15}{41}, \frac{26}{71}, \frac{41}{112})$. This butterfly is presented in Fig. 3.10(c). In Fig. 3.10, the three successive generations of butterflies, clearly shows that the DKT butterfly exhibits self-similarity. We have also observed that the DKT butterfly shares the same number theoretical property as that of the Hofstadter butterfly, even though the two models have no physical similarity.

3.6 Conclusion

We have investigated the double kicked top (DKT) system. Mainly we have compared the properties of the quasienergy spectrum and energy spectrum of the effective Hamiltonian at the high frequency limit. We observe a butterfly like self-similar fractal in the quasienergy spectrum of the DKT system when plotted as a function of one of the system parameters. The butterfly spectrum repeats itself periodically with the increment in that parameter. Since the effective Hamiltonian is obtained perturbatively, we have investigated whether the effective Hamiltonian energy spectrum shares the identical self-similar property. We have observed that this is indeed the case when the energy spectrum is folded to the first Floquet-Brillouin zone and within a certain parameter regime.

We have focused mostly on the parameter regime where the quasienergy spectrum and energy spectrum are H_{eff} folded into the first Floquet-Brillouin zone are very much identical. Therefore, we have studied mostly the energy spectrum of the effective Hamiltonian. Firstly, we have observed the self-similar property in the

DOS of the energy spectrum for a particular irrational value of the system parameter. We have also observed the multifractal properties of the eigenstates of the Floquet Hamiltonian. Besides, we have also observed many localized eigenstates. The most delocalized eigenstate is also a multifractal state.

Then, we have studied the changes in the butterfly spectrum due to the variation of a system parameter. We have observed the disappearance of the butterfly spectrum due to this parameter variation. The disappearance of the butterfly spectrum is systematically studied by comparing the quasienergy spectrum, unfolded energy spectrum of the effective Hamiltonian, and the energy spectrum of the same folded in the first Floquet-Brillouin zone. We have found that the butterfly spectrum formed by the quasienergies and the folded energy spectrum of the effective Hamiltonian show this property of disappearance. On the other hand, we have not observed any disappearance in the butterfly spectrum formed by the unfolded energy spectrum of the effective Hamiltonian. However, we have observed an enhancement in the size of the butterfly without changing its structure.

Finally, we have studied extensively the self-similar property of the butterfly formed by the energy spectrum of the effective Hamiltonian. Unlike previous studies, we have studied the self-similarity of the whole DKT butterfly considering it as a single object. Following the same number theoretical studies performed on the Hofstadter butterfly, we have observed identical looking DKT butterflies in different scales. We have also observed that the DKT butterfly shares many properties with the well known Hofstadter butterfly.